PIP$_3$ controls synaptic function by maintaining AMPA receptor clustering at the postsynaptic membrane

Kristin L. Arendt[1,2,4], **María Royo**[3], **Mónica Fernández-Monreal**[3], **Shira Knafo**[3], **Cortney N. Petrok**[2], **Jeffrey R. Martens**[1,2], and **José A. Esteban**[1,2,3,*]

[1] Neuroscience Program, University of Michigan Medical School, Ann Arbor, Michigan 48109, USA

[2] Department of Pharmacology, University of Michigan Medical School, Ann Arbor, Michigan 48109, USA

[3] Centro de Biología Molecular "Severo Ochoa", Consejo Superior de Investigaciones Científicas (CSIC)/Universidad Autonoma de Madrid, Madrid 28049, Spain

Abstract

Despite their low abundance, phosphoinositides are critical regulators of intracellular signaling and membrane compartmentalization. However, little is known of phosphoinositide function at the postsynaptic membrane. Here we show that continuous synthesis and availability of phosphatidylinositol-(3,4,5)-trisphosphate (PIP$_3$) at the postsynaptic terminal is necessary for sustaining synaptic function in rat hippocampal neurons. This requirement is specific for synaptic, but not for extrasynaptic, AMPA receptors, nor NMDA receptors. We found that PIP$_3$ down-regulation impairs PSD-95 accumulation in spines. Concomitantly, AMPA receptors become more mobile and migrate from the postsynaptic density towards the perisynaptic membrane within the spine, leading to synaptic depression. Interestingly, these effects are only revealed after prolonged inhibition of PIP$_3$ synthesis or by direct quenching of this phosphoinositide at the postsynaptic cell. Therefore, we conclude that a slow, but constant turnover of PIP$_3$ at synapses is required for maintaining AMPA receptor clustering and synaptic strength under basal conditions.

Phosphoinositides (phosphorylated derivatives of phosphatidylinositol) are fundamental second messengers in the cell. They are able to integrate multiple intracellular signaling pathways and modulate a large spectrum of cellular activities[1]. Phosphoinositides are highly compartmentalized in the cell, and in this fashion, they are thought to provide essential spatial and temporal cues for protein recruitment and intracellular membrane trafficking[2]. The functional role of phosphoinositide metabolism and compartmentalization has been

[*]Correspondence should be addressed to J.A.E. (jaesteban@cbm.uam.es): Nicolás Cabrera 1, Madrid 28049, Spain, Phone: +34-91-1964637, Fax: +34-91-1964420.
[4]Current address: Department of Molecular and Cell Biology, University of California at Berkeley, California 94720, USA

studied with great detail at the presynaptic terminal, where phosphoinositide turnover has been shown to be critical for neurotransmitter vesicle cycling and synaptic function[3]. There is also abundant evidence for the relevance of phosphoinositide pathways for synaptic plasticity[4]–[8]. However, very little is known about specific roles of phosphoinositides in membrane trafficking at the postsynaptic terminal, despite the importance of neurotransmitter receptor trafficking for synaptic plasticity[9],[10].

Phosphatidylinositol-(3,4,5)-trisphosphate (PIP_3) is among the most elusive phosphoinositides. Basal levels of PIP_3 are extremely low, due to a tight spatial and temporal regulation of PIP_3 synthesis[11]. Nevertheless, PIP_3 can be found enriched in specific subcellular compartments, such as the tip of growing neurites[12]. Indeed, local accumulation of PIP_3 is very important for the establishment of cell polarity, including neuronal differentiation and dendritic arborization[13],[14]. The mechanisms by which PIP_3 exerts its functions are still being elucidated. Nevertheless, a common theme is the role of PIP_3 as a landmark for docking and co-localization of a variety of signaling molecules at the plasma membrane[1].

AMPA-type glutamate receptors (AMPARs) mediate most excitatory transmission in the brain, and their regulated addition and removal from synapses leads to long-lasting forms of synaptic plasticity such as long-term potentiation (LTP) and long-term depression (LTD)[15]. In addition, AMPARs continuously cycle in and out of the synaptic membrane in a manner that does not require synaptic activity. This constitutive trafficking involves both exocytic delivery from intracellular compartments[16] and fast exchange with surface extrasynaptic receptors *via* lateral diffusion[17]. Still, we know very little about the organization and regulation of AMPARs within the synaptic terminal. In particular, the potential role of PIP_3 in these processes has never been explored.

In this work we have investigated specific actions of PIP_3 at the postsynaptic membrane, using a combination of pharmacological and molecular tools, together with electrophysiology, fluorescence imaging and electron microscopy assays. Surprisingly, we have found that PIP_3 is continuously required for the maintenance of AMPARs at the synaptic membrane. This effect is only visible upon direct PIP_3 quenching or prolonged inhibition of its synthesis, suggesting that a slow but constant turnover of PIP_3 is required for sustaining synaptic function.

RESULTS

PIP_3 limits AMPA receptor-mediated synaptic transmission

As a first step to evaluate the role of PIP_3 in synaptic transmission, we manipulated endogenous PIP_3 levels by overexpressing the pleckstrin homology (PH) domain from General Receptor for Phosphoinositides (GRP1) in CA1 neurons from organotypic hippocampal slice cultures (see Methods). This domain has a 650-fold specificity for PIP_3 *versus* PIP_2 and other phosphoinositides[18], and it has a dominant negative effect on PIP_3-dependent processes by restricting binding to the endogenous targets[19]. As shown in Fig. 1a, this construct (PH-GRP1) is well expressed in neurons, where it reaches dendritic spines. The lack of an obvious membrane distribution of this recombinant protein is consistent with

the presence of very low levels of PIP_3 under basal conditions[11]. That is, PH-GRP1 is expected to be well in excess over endogenous PIP_3[18], as it would be required for PH-GRP1 to act as a dominant negative. Nevertheless, we have confirmed the PIP_3-binding ability and specificity of PH-GRP1 *in vitro* (Fig. 1b,c) and in BHK cells upon PIP_3 up-regulation (Fig. 1d).

We then monitored the effect of PIP_3 quenching with PH-GRP1 on evoked AMPAR- and NMDAR-mediated responses in CA1 pyramidal neurons using whole-cell simultaneous double recordings. Importantly, only CA1 (but not CA3 cells) express the recombinant protein. Therefore, PIP_3 levels are only altered in the postsynaptic cell when monitoring CA3-to-CA1 synaptic transmission. As shown in Fig. 2a, quenching of PIP_3 with PH-GRP1 caused a significant and selective depression of AMPAR synaptic responses compared to control neighboring pyramidal neurons. Recordings at +40mV revealed no effect on NMDAR transmission (for simplicity, only average values are plotted in the graphs, but statistical comparisons are always calculated for infected-uninfected paired data). Importantly, expression of PH-GRP1 did not affect passive membrane properties of the cell, such as holding current or input resistance, indicating that cell-wide ion channel conductances were not altered. In addition, cell size, as reported by whole-cell capacitance was not affected either (Supplementary Fig. 1). Therefore, overnight expression of this construct does not appear to have any general toxic effect in neurons from organotypic slices.

PH domains have been reported to have cellular effects independent from their phosphoinositide binding activity[20]. Therefore, we tested whether the depression of AMPAR transmission by PH-GRP1 was directly due to PIP_3 sequestration. We expressed a PH-GRP1 domain with a point mutation that specifically prevents phosphoinositide binding: R284C[20]. As shown in Fig. 2b, paired recordings for AMPAR-and NMDAR-mediated transmission revealed no difference in synaptic responses between cells expressing PH-GRP1-R284C and their control neighbors. These results confirm that the binding and thus sequestering of PIP_3 causes the depression of AMPAR-mediated transmission.

As an independent approach to test the role of PIP_3 in synaptic transmission, we used specific inhibitors of class I phosphatidylinositol-3-kinases (PI3Ks), the enzymes that generate PIP_3. For these experiments we pre-treated hippocampal slices with 10 μM LY294002 or 100 nM wortmannin for one hour prior to whole-cell recordings (these drugs were also present in the perfusion solution during the recordings). At these concentrations, LY294002 and wortmannin are potent inhibitors of PI3K, without significant effects on phosphoinositide kinases required for $PI(4,5)P_2$ synthesis[11]. Synaptic responses were evoked at −60 mV and +40 mV holding potentials to obtain AMPA/NMDA ratios (Fig. 2c). Compared to the equivalent vehicle control (DMSO), AMPA/NMDA ratio was significantly decreased in cells treated with LY294002 or wortmannin. Finally, depression of AMPA/NMDA ratios was observed in both cultured and acute hippocampal slices (Fig. 2c, right histogram).

To test whether pharmacological inhibition of PI3K and overexpression of PH-GRP1 depress synaptic transmission by the same mechanism, we compared AMPAR and NMDAR

responses between PH-GRP1-expressing and control neurons, after pre-treating the slices with 10 μM LY294002 for 1 hour (LY294002 was also present during the recordings). As shown in Fig. 2d, PH-GRP1 expression did not alter AMPAR nor NMDAR currents with respect to the control neuron when PIP_3 synthesis was inhibited. This result confirms that PH-GRP1 and LY294002 depress synaptic transmission through the same pathway, most likely by limiting PIP_3 availability.

This observed depression of AMPAR-mediated transmission upon PIP_3 depletion suggests that PIP_3 may be a limiting factor for AMPAR synaptic function. If this is the case, enhanced PIP_3 synthesis might lead to increased AMPAR responses. To test this possibility, we generated a constitutively active PI3K by permanently targeting its catalytic subunit (p110) to the plasma membrane using a myristoylation tag (Myr-p110, [21]). The efficacy of this construct to upregulate PIP_3 signaling was confirmed by monitoring Akt phosphorylation in CA1 neurons expressing Myr-p110 (Supplementary Fig. 2). Evoked AMPAR and NMDAR responses were compared between infected and non-infected neighboring pyramidal neurons. Neurons expressing Myr-p110 displayed a significant potentiation of AMPAR transmission (Fig. 2e) with no alteration of NMDAR responses. Passive membrane properties including holding current, input resistance and capacitance were not different between infected and uninfected cells (Supplementary Fig. 1). These results support the interpretation that PIP_3 is a limiting factor controlling AMPAR synaptic function.

Gradual synaptic depression upon PIP_3 synthesis inhibition

Previous reports using PI3K inhibitors have yielded conflicting results on the role of PIP_3 on basal synaptic transmission[4,5]. However, it is important to keep in mind that the magnitude of the decrease in PIP_3 levels upon blockade of its synthesis will depend on its metabolic turnover under basal conditions. Thus, short incubations with PI3K inhibitors may be ineffective if basal PIP_3 turnover is slow. To directly address this possibility, we incubated hippocampal slices with 10 μM LY294002 for up to two hours while monitoring AMPAR synaptic responses using field recordings.

Stable baselines of a minimum of 25 minutes were obtained from hippocampal slices prior to infusion of 10μM LY294002 or 0.05% DMSO (vehicle control). As shown in Fig. 3a,b, slices treated with 10 μM LY294002 displayed a slow and gradual run-down of synaptic transmission, which started to be significant 60–80 min after the onset of PI3K inhibition. In contrast, DMSO-treated slices showed a small decrease in synaptic responses, which was not significant after 2 hours of infusion. As control, treatment with LY294002 did not affect fiber volley amplitude (Fig. 3a,c), suggesting that presynaptic excitability was not altered. Therefore, these results confirm our previous conclusion on the importance of PIP_3 for the maintenance of AMPAR synaptic function. In addition, these data support the interpretation that PIP_3 undergoes a slow turnover under basal conditions, which is only revealed after prolonged inhibition of PIP_3 synthesis (to note, recordings in Fig. 2c started one hour after application of LY294002).

The function of some ion channels has been shown to be directly modulated by phosphoinositides, more typically by PIP_2 (see for example [22]), but also by PIP_3[23]. In order

to test whether this is the case for AMPARs, we recorded extrasynaptic responses evoked by bath application of AMPA (100 nM) from CA1 neurons expressing PH-GRP1 and from neighboring control cells. Recordings were carried out in the presence of 0.5 μM tetrodotoxin (to prevent action potential firing) and 10 μM cyclothiazide (to prevent AMPAR desensitization). As shown in Fig. 3d, whole-cell AMPA-evoked currents were similar in PH-GRP1-expressing neurons and in control neighboring cells. This result suggests that the requirement for PIP_3 is specific for synaptic AMPARs.

Postsynaptic PIP_3 is necessary for long-term potentiation

There have been previous conflicting results on the role of PIP_3 in LTP induction, maintenance or both[4],[5]. However, it is important to note that pharmacological inhibition of PI3K would affect both pre- and postsynaptic cells. In addition, as discussed above, different incubation times with PI3K inhibitors may yield variable depletion of basal PIP_3 levels. In order to circumvent these complications, we decided to test the role of PIP_3 in LTP by directly quenching this phosphoinositide in the postsynaptic cell using PH-GRP1 in organotypic hippocampal slices. Importantly, this experimental manipulation does not affect NMDAR synaptic currents (Fig. 2a), and therefore, it rules out potential effects on LTP induction.

Whole-cell recordings were obtained from neurons expressing PH-GRP1 and from control, uninfected neurons, in an interleaved manner. LTP was induced according to a pairing protocol (see Methods). As shown in Fig. 4a,b, control cells displayed significant potentiation of transmission compared to the unpaired pathway that did not receive LTP-inducing stimulation. In contrast, LTP expression was abolished in cells expressing PH-GRP1 (black symbols in panel A; black column in panel B).

PIP_3 requirements for cycling and regulated AMPA receptors

Most AMPARs in the hippocampus are composed of GluA1/GluA2 or GluA3/GluA2 subunit combinations[24] (subunit nomenclature according to [25]). These two populations appear to reach their synaptic targets according to different pathways, with GluA2/3 continuously cycling in and out of synapses and GluA1-containing receptors undergoing acute, activity-dependent synaptic delivery[26] (but see also [27]). Therefore, we decided to separately test the PIP_3 requirements of these two populations.

To this end, we co-expressed individual EGFP-tagged AMPAR subunits with either RFP or an RFP-tagged PH-GRP1 in organotypic slice cultures using the biolistic delivery system (see Methods). When overexpressed, these subunits form homomeric receptors, which can be detected at synapses from their inward rectification properties[28],[29] (in the case of GluA2, we used the unedited version R607Q). Recombinant GluA2 receptors behave as endogenous GluA2/3 heteroligomers[28]; thus, they can be used to monitor the constitutively cycling population of AMPARs. When GluA2(R607Q) was expressed with RFP, the rectification index was significantly increased compared to non-transfected cells (Fig. 4c; compare first and second columns), indicating presence of the recombinant receptor at the synapse. In contrast, when GluA2(R607Q) was coexpressed with PH-GRP1, this increase in

rectification was abolished (Fig. 4c; compare second and third columns), indicating that PIP$_3$ is needed for the delivery and/or stability of this population of AMPARs at synapses.

Similar assays were carried out with recombinant GluA1 subunits to monitor the activity-regulated population of AMPARs[29]. GluA1 is driven into synapses when co-expressed with a constitutively-active form of αCaMKII (tCaMKII), as judged from the increase in the rectification index (Fig. 4c, compare first and fourth columns). However, when PH-GRP1 is co-expressed with GluA1 and tCaMKII, this increase in rectification is not observed (Fig. 4c; compare fourth and fifth columns). This finding suggests that PIP$_3$ is also necessary for the synaptic presence of this population of AMPARs. These results were essentially replicated using the PI3K inhibitor LY294002 (10 μM) on hippocampal slices expressing either GluA2(R607Q) or GluA1 plus tCaMKII (Fig. 4d).

These experiments using recombinant receptors fit very well with our results monitoring endogenous AMPARs during basal synaptic transmission and LTP. Together, these data strongly suggest that PIP$_3$ is a common requirement for all populations of AMPARs.

AMPA receptor accumulation at spines upon PIP$_3$ depletion

The results described above suggest that PIP$_3$ availability affects synaptic, but not extrasynaptic AMPARs. Therefore, we hypothesized that PIP$_3$ may play a local role in AMPAR function at synapses. To address this hypothesis, we evaluated the distribution of AMPARs at dendritic spines upon PIP$_3$ depletion.

We used biolistic gene delivery to co-express EGFP-tagged GluA2 together with either RFP (control) or an RFP-tagged PH-GRP1, in organotypic hippocampal slices. The partition of GluA2 between spines and dendrites was estimated from the intensity of the GFP signal in the spine head versus the adjacent dendritic shaft (see Methods). Similarly, the surface distribution of the recombinant receptor in spines and dendrites was assessed by immunostaining with an anti-GFP coupled to an infrared fluorophore (Cy5) under non-permeabilized conditions (the GFP tag is placed at the extracellular N terminus of the receptor; see Fig. 5a for examples and Supplementary Fig. 3 for a control of the non-permeabilizing conditions for surface immunostaining).

As shown in Fig. 5b, GluA2 partitions almost equally between the spine head and the adjacent dendrite when expressed with RFP. To our surprise, co-expression with PH-GRP1 led to a small, but significant increase in the amount of GluA2 receptor in the spine (Fig. 5b, left pair of columns). Notably, PH-GRP1 produced a similar accumulation of GluA2 at the plasma membrane (surface) of the spine (Fig. 5b, right pair of columns). This redistribution appears to be local, since long-range distribution of GluA2 along the primary apical dendrite was not altered by PH-GRP1 expression (Supplementary Fig. 4). These results were replicated using a pharmacological approach to inhibit PIP$_3$ synthesis (10 μM LY294002; Fig. 5c).

Importantly, spine size (estimated from cytosolic GFP distribution) and distribution of the PIP$_3$ precursor, phosphatidylinositol-(4,5)-bisphosphate (PIP$_2$) at spines were not altered upon PIP$_3$ blockade (Supplementary Fig. 5). Therefore, these combined data indicate that

PIP$_3$ depletion leads to a local redistribution of AMPARs, which unexpectedly, accumulate in spines. As will be shown below, ultrastructural analyses indicated that this receptor accumulation occured preferentially on the extrasynaptic region of the spine plasma membrane (Fig. 7).

PIP$_3$ contributes to PSD-95 accumulation in spines

PSD-95 is a synaptic scaffolding molecule that critically controls the accumulation of AMPARs at synapses[30], and accordingly, it is a determining factor for the maintenance of synaptic strength[31–33]. Therefore, we decided to test whether PIP$_3$ may affect PSD-95 accumulation at synapses. To this end, we co-expressed GFP-tagged PSD-95 with plain (cytosolic) RFP or with RFP-PH-GRP1 in CA1 neurons from organotypic slice cultures (see Fig. 6a for representative examples). The accumulation of PSD-95 in spines was then quantified from the ratio of GFP fluorescence at the spine head *versus* the adjacent dendritic shaft.

As shown in Fig. 6b, co-expression with PH-GRP1 significantly reduced the accumulation of PSD-95 in spines, as compared with RFP-expressing neurons. This reduction was detected across the whole population of spines (left shift in the cumulative distribution). Importantly, as mentioned earlier, PIP$_3$ depletion did not alter spine size (Supplementary Fig. 5a). Therefore, these results strongly suggest that PIP$_3$ availability is important for PSD-95 enrichment in spines.

PIP$_3$ regulates AMPA receptor mobility at the spine surface

PSD-95 is a critical factor for the stability of AMPARs at the synaptic membrane[30]. Therefore, the results shown above suggest that the depression of synaptic strength upon PIP$_3$ depletion may be due to a reduction in PSD-95-mediated anchoring of AMPARs at synapses. As an initial approach to test this hypothesis, we evaluated the mobility of AMPARs at the surface of dendritic spines using fluorescence recovery after photobleaching (FRAP) and Super-Ecliptic-pHluorin-tagged GluA2 (SEP-GluA2). Super-ecliptic-pHluorin is a highly pH-sensitive version of GFP, which has been previously used to track surface AMPARs[34].

SEP-GluA2 receptors were expressed in organotypic hippocampal slices, and PIP$_3$ levels were reduced by treatment with the PI3K inhibitor LY294002. Spines expressing SEP-GluA2 were photobleached and the extent of fluorescence recovery was measured over 30 minutes (see representative examples in Fig. 6c). As shown in Fig. 6d, approximately 25% of the SEP-GluA2 signal is recovered in the spine over a time course of 5–10 min (time constant of 5.7 min). In contrast, in slices treated with LY294002, SEP-GluA2 fluorescence recovered to a significantly greater extent (around 50%) over a similar time course (time constant of 5.9 min). These results indicate that PIP$_3$ depletion leads to an increase in the fraction of AMPARs that are free to exchange between the dendrite and the spine. As a control, the mobility of a membrane-anchored version of GFP (GFP with the farnesylation sequence of H-Ras) was not altered by LY294002 (Supplementary Fig. 6). In addition, PIP$_3$ depletion did not change the mobility of SEP-GluA2 in dendrites (Supplementary Fig. 7). Therefore, these combined observations indicate that PIP$_3$ specifically modulates the flow of

AMPARs between the spine and the dendrite, in a manner that is consistent with a decreased stability of receptors at the synaptic membrane in the absence of PIP_3.

PSD-95 anchors AMPARs at synapses through its interaction with transmembrane AMPAR regulatory proteins (TARPs)[30,31]. We then tested whether PIP_3 is required for PSD-95/ TARP interaction. To this end, we inhibited PIP_3 synthesis in hippocampal slices with LY294002 for 2 hours, prepared total protein extracts, and carried out co-immunoprecipitations between PSD-95 and two major TARPs expressed in the hippocampus: γ-8 and γ-2 (stargazin)[35]. As shown in Supplementary Fig. 8, PSD-95 can be immunoprecipitated with both γ-8 and γ-2 from hippocampal extracts. Surprisingly, this interaction appeared to be stronger in slices pre-treated with LY294002. The mechanism for this unexpected strengthening of PSD-95/TARP interaction upon PIP_3 depletion is unclear. Nevertheless, we can conclude that the depression of synaptic responses and increased mobility of surface AMPARs induced by PIP_3 depletion are not due to an impaired interaction between PSD-95 and TARPs.

Local rearrangement of AMPA receptors at the spine surface

One of the most surprising results of this work is that AMPARs accumulate at the spine plasma membrane upon PIP_3 depletion (Fig. 5), although synaptic transmission is depressed (Figs. 2 and 3). However, it should be kept in mind that only a small fraction (around 15%) of the spine plasma membrane is actually occupied by the postsynaptic density, where excitatory transmission occurs[36]. At this submicron scale, confocal fluorescence microscopy cannot easily resolve whether receptors present on the spine surface are actually located on the synaptic membrane. To directly evaluate whether PIP_3 affects AMPAR clustering at the postsynaptic membrane, we employed post-embedding immunogold electron microscopy. In addition to its high spatial resolution, this technique has the advantage of monitoring endogenous AMPARs.

Hippocampal slices were treated with 10 μM LY294002 (or DMSO, as control), and processed for postembedding immunogold detection using anti-GluA2 antibodies (see Methods). Electron micrographs were sampled randomly from excitatory (asymmetric) synapses in the stratum radiatum (CA1) (see representative images in Fig. 7a). The abundance of anti-GluA2 immunogold particles was quantified at three compartments: the postsynaptic density, the extrasynaptic membrane lateral to the PSD and the intracellular space within the spine. Interestingly, slices treated with LY294002 displayed a significant accumulation of GluA2 particles in the extrasynaptic membrane lateral to the PSD (Fig. 7b). This effect was accompanied by a decrease in the PSD population, resulting in no net change in total membrane localization (PSD plus extrasynaptic membrane) *versus* intracellular fraction (Fig. 7b).

Prompted by this result, we took a closer inspection to the distribution of GluA2 along the synaptic and perisynaptic membrane within the spine. To this end, we measured the lateral distance of each individual gold particle in these two compartments with respect to the closest PSD edge. Particles within the extrasynaptic membrane are given positive distances (larger numbers representing particles farther away from the PSD edge) and particles within the PSD are given ne gative distances (larger numbers representing particles closer to the

center of the PSD). As shown in Fig. 7c,d, under control conditions, AMPARs accumulate to higher densities within the PSD membrane, whereas the perisynaptic membrane near the PSD edge remains rather unpopulated by receptors. In contrast, upon PIP$_3$ depletion, the distribution of AMPARs becomes much more homogeneous along synaptic and extrasynaptic membrane within the spine: AMPAR immunolabeling decreases at the PSD and increases in the perisynaptic membrane (Fig. 7c), to the point that receptor density does not appreciably change across the PSD edge (see cumulative distributions in Fig. 7d). Similar results were obtained with a different antibody monitoring the GluA3 subunit of AMPARs (Supplementary Fig. 9). Therefore, this analysis confirms that PIP$_3$ depletion leads to a very local redistribution of AMPARs within the spine surface, which results in a decreased receptor density at the synaptic membrane and an increased receptor accumulation on the extrasynaptic surface of the spine.

Importantly, this result monitoring endogenous receptors is consistent with the depression of AMPAR synaptic responses produced by PH-GRP1 expression or LY294002 treatment (Figs. 2 and 3), and it also fits with the increased fraction of mobile recombinant receptors reported by FRAP measurements (Fig. 6) (receptors on the perisynaptic membrane exchange more readily with extrasynaptic receptors than those at the postsynaptic site[17]). Taken together, these results indicate that PIP$_3$ has a critical role in the subsynaptic distribution and dynamics of AMPARs, which bears direct consequences for the maintenance of synaptic function.

Electrophysiological detection of perisynaptic receptors

In order to functionally evaluate the presence of perisynaptic AMPARs induced by PIP$_3$ depletion, we decided to test the effect of PH-GRP1 on synaptic responses elicited in the presence of a glutamate reuptake blocker. The rationale is that synaptically released glutamate may reach these nearby receptors if neurotransmitter reuptake is inhibited. To this end, we pre-incubated slices with the glutamate uptake blocker L-trans-pyrrolidine-2,4-dicarboxylate (L-t-PDC). This is a potent uptake inhibitor that does not have any direct action on glutamate receptors[37]. In the presence of L-t-PDC, AMPAR-mediated synaptic responses from neurons expressing PH-GRP1 were no longer depressed with respect to control neurons (see Fig. 8a). This result supports our interpretation that PIP$_3$ depletion leads to AMPAR diffusion into the perisynaptic membrane of the spine.

Nevertheless, the effects of blocking neurotransmitter reuptake are not necessarily straightforward. It has been previously reported that inhibition of glutamate uptake produces depression of basal synaptic transmission in primary neuronal cultures[38] and in hippocampal slices[39] (but see also [40]). This depression is thought to be mediated by the activation of metabotropic glutamate receptors[38]. Indeed, we observed a run-down of basal synaptic transmission in control neurons when perfusing L-t-PDC (Fig. 8b; white symbols). In the case of PIP$_3$-depleted neurons (PH-GRP1), this depression was greatly reduced or completely absent (Fig. 8b, black symbols). This result is consistent with the additional contribution of nearby extrasynaptic receptors in these neurons, which would compensate from the depression otherwise induced by blocking glutamate uptake. Since PH-GRP1 neurons start from an already depressed situation (Fig. 2a), by the end of the incubation with

L-t-PDC they display similar AMPAR responses as to those from control neurons (see Fig. 8b, inset, for a representative pair of infected and uninfected neurons recorded simultaneously).

Regardless of the macroscopic effects of L-t-PDC on basal synaptic transmission, the fact that blockade of glutamate uptake abolishes the depression induced by PIP_3 depletion strongly supports the interpretation that AMPARs redistribute to the nearby perisynaptic membrane in the absence of PIP_3.

DISCUSSION

In this manuscript we have shown that PIP_3 is a critical effector of AMPAR synaptic function and plasticity, and that it is required for the maintenance of synaptic strength. In particular, we have found that PIP_3 down-regulation leads to a depression of synaptic transmission, which is specific for synaptic AMPARs, since it does not affect NMDAR nor extrasynaptic AMPAR currents. Interestingly, PIP_3 seems to act at a very local scale, by ensuring PSD-95-mediated clustering of AMPARs at the postsynaptic membrane, and therefore, preventing receptor dispersion into the neighboring extrasynaptic membrane of the spine. In addition, PIP_3 depletion leads to the accumulation of AMPARs in spines, possibly through a separate mechanism that remains to be characterized.

These results clarify previous conflicting reports on the role of PIP_3 signaling for synaptic function and plasticity. We report for the first time that basal levels of PIP_3 at the postsynaptic terminal are necessary for sustaining synaptic function. Importantly, this requirement is only unmasked when blocking PI3K activity for long periods of time (> 1 hour), suggesting that PIP_3 levels (at least at synapses) are subject to a slow turnover. This is an important finding for synaptic signaling, since it implies that both synthetic (PI3K) and degradative (PTEN and/or SHIP) activities are present in unstimulated neurons. Our results suggest that, under basal conditions, these activities are tuned to maintain low (but physiologically relevant) levels of PIP_3. Obviously, this interpretation also includes the possibility of fast regulation of PIP_3 levels during plasticity. In fact, LTP induction and NMDAR activation have been previously reported to trigger the PI3K signaling cascade [41],[42]. According to this scenario, acute blockade of PI3K during LTP induction should be sufficient to prevent the fast up-regulation of PIP_3 and synaptic potentiation. However, prolonged blockade of PIP_3 synthesis would be needed to unveil its requirement for the maintenance of synaptic transmission.

How is PI3K activity maintained (even if at low levels) under basal conditions? This is an important point, since PI3K is usually seen as a regulated enzyme that is activated by upstream effectors (receptor protein tyrosine kinases, G protein coupled receptors, etc.; see [1] for a review). However, it is worth noting that most PI3K activating mechanisms operate by recruiting the enzyme to the plasma membrane, where its substrate, PIP_2, is found. In fact, "passive" targeting of PI3K to the plasma membrane (in the absence of receptor stimulation) leads to a constitutive up-regulation of PIP_3 signaling[21] (see also Supplementary Fig. 2). Interestingly, it has been shown that PI3K is localized at excitatory synapses, and that it directly binds the cytosolic C-terminus of the AMPAR[6]. This interaction is constitutive and

preserves the catalytic activity of PI3K[6]. Therefore, we propose that, *via* its association to AMPARs, PI3K would be maintained in close proximity to the synaptic membrane, where it would responsible for supplying a low but constant level of PIP$_3$ necessary to sustain synaptic transmission.

Why is PIP$_3$ constantly needed at the postsynaptic membrane? To some extent, this situation is reminiscent of the presence of PIP$_3$ in subcellular domains with high membrane dynamics, such as the tip of growing neurites[12]. Although the precise role of PIP$_3$ in this process is far from clear, a recurring theme is the requirement of PIP$_3$ for the establishment or maintenance of cell membrane polarity[12]–[14]. We now know that the postsynaptic terminal is indeed a domain of intense and polarized membrane dynamics, which is critical for both synaptic function maintenance and plasticity[10]. Therefore, our results suggest that a slow, but active, turnover of PIP$_3$ may be critical for subserving basal membrane dynamics constantly operating at the postsynaptic terminal.

Finally, our data indicate that PIP$_3$ plays a very distinct and local function for the regulation of AMPARs at synapses. Specifically, we have found that PIP$_3$ contributes to the accumulation of PSD-95 at spines. Accordingly, PIP$_3$ depletion produces an enhanced mobility of AMPARs in spines, which is accompanied by receptor dispersion into the perisynaptic membrane. Therefore, our results suggest that PIP$_3$ is a critical factor for the synaptic retention of AMPARs, perhaps *via* modulation of the PSD-95 synaptic scaffold. This mechanism is likely to be specific for AMPARs, since knockdown of PSD-95 does not significantly alter synaptic NMDARs[43]. The mechanistic link between PIP$_3$ and PSD-95 remains to be elucidated. It has been recently shown that a variety of PDZ domains and polybasic clusters confer phosphoinosotide binding specificity[44]–[46]. Therefore, the recruitment of PSD-95 into spines may be modulated by a complex network of phosphoinositide-dependent interactions.

In summary, this work has offered new insights into the complex interplay between lipids and neurotransmitter receptors for the regulation of synaptic function. In addition, it has revealed that an important but poorly understood phosphoinositide, phosphatidylinositol-(3,4,5)-trisphosphate, is a critical factor for the local concentration of AMPARs at the postsynaptic membrane.

METHODS

Materials

The PI3K inhibitors LY294002 and wortmannin, and the glutamate uptake inhibitor L-*Trans*-pyrrolidine-2,4-dicarboxylate (L-t-PDC) were from Sigma. The antibodies used in this study were: anti-GFP (Roche); GluR2, GluR3, phospho-Akt (Thr308) and stargazin (Millipore); Akt (Cell Signaling); TARP γ-8 (Frontier Science, Hokkaido, Japan).

Construction of recombinant proteins and expression

The coding sequence of the pleckstrin homology (PH) domain of GRP1 was amplified by RT-PCR from rat brain mRNA and cloned downstream of the enhanced GFP (Clontech) (EGFP-PH-GRP1) or the red fluorescence protein variant tdimer2[47] (RFP-PH-GRP1). The

corresponding point mutant abolishing PIP$_3$ binding, R284C[20], was introduced by PCR-directed mutagenesis. The PH domain of human phospholipase C-δ1 fused to EGFP was obtained from Dr. Ronald Holz (PH-PLC-EGFP). A constitutively active form of PI3K was generated by adding an N-terminal myristoylation sequence to the catalytic domain (p110α) of mouse PI3K, as previously described[21]. This construct was then tagged with enhanced GFP (Clontech) at the C-terminus (Myr-p110-EGFP). The EGFP-tagged AMPAR subunits (GluA1-EGFP and GluA2-R607Q-EGFP), PSD-95 and the truncated αCaMKII construct (tCaMKII) were prepared as previously described[28],[32]. The membrane-anchored form of GFP was obtained from Carlos Dotti. In this construct, the EGFP coding sequence is followed by a 21-aa farnesylation signal from H-Ras (pEGFP-CAAX). The pH-sensitive Super-Ecliptic-pHluorin-GluA2 construct was obtained from Roberto Malinow[34]. All these constructs were recloned in pSinRep5 for expression using Sindbis virus. Organotypic cultures of hippocampal slices were prepared from postnatal day 5–6 rats. After 4–5 days in culture, the recombinant gene is delivered into the slices using Sindbis virus or biolistic gene deliver ("gene gun"). Protein expression was typically for 15 h or for 1.5 days when expressing AMPAR subunits. All biosafety procedures and animal care protocols were approved by the University of Michigan Committee on Use and Care of Animals and the bioethics committee from the Consejo Superior de Investigaciones Cientificas (CSIC).

Protein extracts and immunoprecipitations

Protein extracts from hippocampal slices were prepared in 10 mM HEPES, 150 mM NaCl, 10 mM EDTA, 0.1 mM phenylmethanesulphonylfluoride (PMSF), 2 μg/ml of chymostatin, leupeptin, antipain and pepstatin, and 1 % Triton X-100. For immunoprecipitations, 200–300 μg of protein extracts were incubated with 5 μg of the corresponding antibody and with 40 μl of protein G-sepharose beads (50%) (Amersham Biosciences), for 4 hours at 4°C. Samples were then washed and immunoprecipitated proteins were eluted by boiling in 1× Laemmli sample buffer and separated by SDS-PAGE. Visualization of immunoprecipitated proteins was done by Western Blot and chemiluminescence.

In vitro phosphoinositide binding assays

PIP pull-down assay—Different PH-domain EGFP fusion proteins were expressed in organotypic hippocampal slice cultures using the Sindbis virus. Slices were then homogenized in a buffer containing 10 mM HEPES pH 7.4, 150 mM NaCl, 0.5% Nonidet P-40, 5 mM DTT, 0.1 mM PMSF, 10 μg/μL chymostatin, 10 μg/μL leupeptin, 10 μg/μL antipain, 10 μg/μL pepstatin. Insoluble extracts were removed via high-speed centrifugation (1 min, 13,200 rpm). The supernatants are then incubated for 3 hours at 4°C with PI(4,5)P$_2$- or PI(3,4,5)P$_3$-coated agarose beads, or with control, uncoated beads (Echelon). Bound and unbound fractions are then separated by centrifugation (pull-down). The presence of the different PH domains in the bound fractions was tested by western blot using anti-GFP antibodies.

PIP membrane overlay assay—Different PH domains fused to EGFP were expressed in BHK cells *via* Sindbis virus. Whole-cell extracts are then prepared in 1% non-fat dry milk dissolved in PBS with 0.1% Tween-20. Insoluble material is removed by centrifugation. Protein extracts are applied on phosphoinositide strips (Echelon) and incubated for 2 hours

at room temperature. The phosphoinositide strips are then washed with PBS-Tween and incubated with anti-GFP for detection of bound recombinant proteins.

Electrophysiology

Voltage-clamp simultaneous whole-cell recordings are obtained from nearby pairs of infected and uninfected (control) CA1 pyramidal neurons, under visual guidance using fluorescence and transmitted light illumination. The recording chamber is perfused with 119 mM NaCl, 2.5 mM KCl, 4 mM $CaCl_2$, 4 mM $MgCl_2$, 26 mM $NaHCO_3$, 1 mM NaH_2PO_4, 11 mM glucose, 0.1 mM picrotoxin, and 4 μM 2-chloroadenosine, at pH 7.4, gassed with 5% CO_2/95% O_2. Patch recording pipettes (3–6 MΩ) are filled with 115 mM cesium methanesulfonate, 20 mM CsCl, 10 mM HEPES, 2.5 mM $MgCl_2$, 4 mM Na_2ATP, 0.4 mM Na_3GTP, 10 mM sodium phosphocreatine, and 0.6 mM EGTA at pH 7.25. Synaptic responses are evoked with bipolar electrodes using single-voltage pulses (200 μs, up to 20 V). The stimulating electrodes are placed over Schaffer collateral fibers between 300 and 500 μm from the recorded cells. Because only CA1 cells (and not CA3 cells) are infected, this configuration ensures that recombinant proteins are always expressed exclusively in the postsynaptic cell. Synaptic AMPAR-mediated responses are measured at −60 mV and NMDA receptor (NMDAR)-mediated responses at +40 mV, at a latency when AMPAR responses have fully decayed (60 ms). For rectification studies, AMPAR responses were recorded at −60 mV and +40 mV in the presence of 0.1 mM D,L-2-amino-5-phosphonovaleric acid (APV) in the perfusion solution and 0.1 mM spermine in the intracellular solution. The rectification index is calculated as the ratio between the AMPAR synaptic response at −60 mV and +40 mV. Synaptic responses are averaged over 50–100 trials. LTP was induced using a pairing protocol by stimulating Schaffer collateral fibers at 3 Hz (540 pulses) while depolarizing the postsynaptic cell to 0 mV. Field excitatory postsynaptic potentials (fEPSPs) were acquired with 2.5 M NaCl in the recording pipette. All electrophysiological recordings were carried out with Multiclamp 700A/B amplifiers (Axon Instruments).

Confocal fluorescence imaging

Fluorescence images were acquired with an Olympus FV500 confocal microscope and a 63x lens using FluoView software. Surface immunostaining for EGFP-tagged AMPAR subunits was carried out under nonpermeabilized conditions using anti-GFP (Roche) and biotinylated anti-mouse (Sigma) antibodies, and streptavidin coupled to Cy5 (Amersham Biosciences) (detergents were omitted in all incubations). Image analysis was carried out with Image J. Briefly, line plots of fluorescence intensity were generated across spine heads and the adjacent dendritic shafts. Fluorescence intensity at each compartment was quantified from the peaks corresponding to the spine and the dendrite after background subtraction. Spine/dendrite ratios were calculated from these values. This method is internally normalized for immunostaining variability, since immunofluorescence values are always acquired in pairs of spine and adjacent dendrite. Additionally, spine-dendrite pairs are always selected from the GFP channel, avoiding any bias with respect to their surface immunostaining.

For fluorescence recovery after photobleaching (FRAP) experiments, GFP signal from dendritic spines or specific dendritic regions was photobleached with high laser intensity for

5 seconds. Recovery of fluorescence was measured at different time intervals after photobleaching. Fluorescence values at the bleached area are normalized to those at an adjacent "non-bleached" region, to compensate for ongoing bleaching during imaging.

Postembedding immunogold

Hippocampal slices were fixed and processed for osmium-free post-embedding immunogold labeling essentially as described previously[48]. AMPARs were labeled with anti-GluA2 or -GluA3 antibodies (Millipore), and secondary antibodies coupled to 10-nm gold particles (Electron Microscopy Sciences). Electron micrographs were obtained with a Philips CM-100 transmission electron microscope and a Kodak 1.6 Megaplus digital camera. Quantification of gold particles and distance measurements were performed onthe digital images using Image J software.

Statistical analyses

All graphs represent average values ± s.e.m. Statistical differences were calculated according to nonparametric tests. Comparisons between multiple groups were performed with the Kruskal-Wallis ANOVA. When significant differences were observed, p values for pairwise comparisons were calculated according to two-tailed Mann-Whitney tests (for unpaired data) or Wilcoxon tests (for paired data). Comparisons between cumulative distributions (Figs. 6b, 7d and Supplementary Fig. 9c) were performed according to two-sample Kolmogorov–Smirnov tests. p values are indicated in each figure.

Supplementary Material

Refer to Web version on PubMed Central for supplementary material.

Acknowledgments

References

1. Cantley LC. The phosphoinositide 3-kinase pathway. Science. 2002; 296:1655–7. [PubMed: 12040186]

2. Di Paolo G, De Camilli P. Phosphoinositides in cell regulation and membrane dynamics. Nature. 2006; 443:651–7. [PubMed: 17035995]

3. Wenk MR, De Camilli P. Protein-lipid interactions and phosphoinositide metabolism in membrane traffic: insights from vesicle recycling in nerve terminals. Proc Natl Acad Sci U S A. 2004; 101:8262–9. [PubMed: 15146067]

4. Sanna PP, et al. Phosphatidylinositol 3-kinase is required for the expression but not for the induction or the maintenance of long-term potentiation in the hippocampal CA1 region. J Neurosci. 2002; 22:3359–65. [PubMed: 11978812]

5. Opazo P, Watabe AM, Grant SG, O'Dell TJ. Phosphatidylinositol 3-kinase regulates the induction of long-term potentiation through extracellular signal-related kinase-independent mechanisms. J Neurosci. 2003; 23:3679–88. [PubMed: 12736339]

6. Man HY, et al. Activation of PI3-kinase is required for AMPA receptor insertion during LTP of mEPSCs in cultured hippocampal neurons. Neuron. 2003; 38:611–24. [PubMed: 12765612]

7. Qin Y, et al. State-dependent Ras signaling and AMPA receptor trafficking. Genes Dev. 2005; 19:2000–15. [PubMed: 16107614]

8. Horne EA, Dell'Acqua ML. Phospholipase C is required for changes in postsynaptic structure and function associated with NMDA receptor-dependent long-term depression. J Neurosci. 2007; 27:3523–34. [PubMed: 17392468]

9. Shepherd JD, Huganir RL. The cell biology of synaptic plasticity: AMPA receptor trafficking. Annu Rev Cell Dev Biol. 2007; 23:613–43. [PubMed: 17506699]

10. Kennedy MJ, Ehlers MD. Organelles and trafficking machinery for postsynaptic plasticity. Annu Rev Neurosci. 2006; 29:325–62. [PubMed: 16776589]

11. Vanhaesebroeck B, et al. Synthesis and function of 3-phosphorylated inositol lipids. Annu Rev Biochem. 2001; 70:535–602. [PubMed: 11395417]

12. Menager C, Arimura N, Fukata Y, Kaibuchi K. PIP3 is involved in neuronal polarization and axon formation. J Neurochem. 2004; 89:109–18. [PubMed: 15030394]

13. Jaworski J, Spangler S, Seeburg DP, Hoogenraad CC, Sheng M. Control of dendritic arborization by the phosphoinositide-3′-kinase-Akt-mammalian target of rapamycin pathway. J Neurosci. 2005; 25:11300–12. [PubMed: 16339025]

14. Kumar V, Zhang MX, Swank MW, Kunz J, Wu GY. Regulation of dendritic morphogenesis by Ras-PI3K-Akt-mTOR and Ras-MAPK signaling pathways. J Neurosci. 2005; 25:11288–99. [PubMed: 16339024]

15. Malinow R, Malenka RC. AMPA receptor trafficking and synaptic plasticity. Annu Rev Neurosci. 2002; 25:103–26. [PubMed: 12052905]

16. Gerges NZ, Backos DS, Rupasinghe CN, Spaller MR, Esteban JA. Dual role of the exocyst in AMPA receptor targeting and insertion into the postsynaptic membrane. Embo J. 2006; 25:1623–34. [PubMed: 16601687]

17. Tardin C, Cognet L, Bats C, Lounis B, Choquet D. Direct imaging of lateral movements of AMPA receptors inside synapses. Embo J. 2003; 22:4656–65. [PubMed: 12970178]

18. Klarlund JK, Tsiaras W, Holik JJ, Chawla A, Czech MP. Distinct polyphosphoinositide binding selectivities for pleckstrin homology domains of GRP1-like proteins based on diglycine versus triglycine motifs. J Biol Chem. 2000; 275:32816–21. [PubMed: 10913124]

19. Helms MN, et al. Phosphatidylinositol 3,4,5-trisphosphate mediates aldosterone stimulation of epithelial sodium channel (ENaC) and interacts with gamma-ENaC. J Biol Chem. 2005; 280:40885–91. [PubMed: 16204229]

20. Varnai P, et al. Selective cellular effects of overexpressed pleckstrin-homology domains that recognize PtdIns(3,4,5)P3 suggest their interaction with protein binding partners. J Cell Sci. 2005; 118:4879–88. [PubMed: 16219693]

21. Klippel A, et al. Membrane localization of phosphatidylinositol 3-kinase is sufficient to activate multiple signal-transducing kinase pathways. Mol Cell Biol. 1996; 16:4117–27. [PubMed: 8754810]

22. Wu L, Bauer CS, Zhen XG, Xie C, Yang J. Dual regulation of voltage-gated calcium channels by PtdIns(4,5)P2. Nature. 2002; 419:947–52. [PubMed: 12410316]

23. Tong Q, Gamper N, Medina JL, Shapiro MS, Stockand JD. Direct activation of the epithelial Na(+) channel by phosphatidylinositol 3,4,5-trisphosphate and phosphatidylinositol 3,4-bisphosphate produced by phosphoinositide 3-OH kinase. J Biol Chem. 2004; 279:22654–63. [PubMed: 15028718]

24. Wenthold RJ, Petralia RS, Blahos J II, Niedzielski AS. Evidence for multiple AMPA receptor complexes in hippocampal CA1/CA2 neurons. J Neurosci. 1996; 16:1982–9. [PubMed: 8604042]

25. Collingridge GL, Olsen RW, Peters J, Spedding M. A nomenclature for ligand-gated ion channels. Neuropharmacology. 2009; 56:2–5. [PubMed: 18655795]

26. Malinow R, Mainen ZF, Hayashi Y. LTP mechanisms: from silence to four-lane traffic. Curr Opin Neurobiol. 2000; 10:352–7. [PubMed: 10851179]

27. Lu W, et al. Subunit composition of synaptic AMPA receptors revealed by a single-cell genetic approach. Neuron. 2009; 62:254–68. [PubMed: 19409270]

28. Shi S, Hayashi Y, Esteban JA, Malinow R. Subunit-specific rules governing AMPA receptor trafficking to synapses in hippocampal pyramidal neurons. Cell. 2001; 105:331–43. [PubMed: 11348590]

29. Hayashi Y, et al. Driving AMPA receptors into synapses by LTP and CaMKII: requirement for GluR1 and PDZ domain interaction. Science. 2000; 287:2262–7. [PubMed: 10731148]

30. Bats C, Groc L, Choquet D. The interaction between Stargazin and PSD-95 regulates AMPA receptor surface trafficking. Neuron. 2007; 53:719–34. [PubMed: 17329211]

31. Schnell E, et al. Direct interactions between PSD-95 and stargazin control synaptic AMPA receptor number. Proc Natl Acad Sci U S A. 2002; 99:13902–7. [PubMed: 12359873]

32. Ehrlich I, Malinow R. Postsynaptic density 95 controls AMPA receptor incorporation during long-term potentiation and experience-driven synaptic plasticity. J Neurosci. 2004; 24:916–27. [PubMed: 14749436]

33. Stein V, House DR, Bredt DS, Nicoll RA. Postsynaptic density-95 mimics and occludes hippocampal long-term potentiation and enhances long-term depression. J Neurosci. 2003; 23:5503–6. [PubMed: 12843250]

34. Kopec CD, Li B, Wei W, Boehm J, Malinow R. Glutamate receptor exocytosis and spine enlargement during chemically induced long-term potentiation. J Neurosci. 2006; 26:2000–9. [PubMed: 16481433]

35. Tomita S, et al. Functional studies and distribution define a family of transmembrane AMPA receptor regulatory proteins. J Cell Biol. 2003; 161:805–16. [PubMed: 12771129]

36. Harris KM, Jensen FE, Tsao B. Three-dimensional structure of dendritic spines and synapses in rat hippocampus (CA1) at postnatal day 15 and adult ages: implications for the maturation of synaptic physiology and long-term potentiation. JNeurosci. 1992; 12:2685–705. [PubMed: 1613552]

37. Bridges RJ, Stanley MS, Anderson MW, Cotman CW, Chamberlin AR. Conformationally defined neurotransmitter analogues. Selective inhibition of glutamate uptake by one pyrrolidine-2,4-dicarboxylate diastereomer. J Med Chem. 1991; 34:717–25. [PubMed: 1671706]

38. Maki R, Robinson MB, Dichter MA. The glutamate uptake inhibitor L-trans-pyrrolidine-2,4-dicarboxylate depresses excitatory synaptic transmission via a presynaptic mechanism in cultured hippocampal neurons. J Neurosci. 1994; 14:6754–62. [PubMed: 7965076]

39. Li S, et al. Soluble oligomers of amyloid Beta protein facilitate hippocampal long-term depression by disrupting neuronal glutamate uptake. Neuron. 2009; 62:788–801. [PubMed: 19555648]

40. Isaacson JS, Nicoll RA. The uptake inhibitor L-trans-PDC enhances responses to glutamate but fails to alter the kinetics of excitatory synaptic currents in the hippocampus. J Neurophysiol. 1993; 70:2187–91. [PubMed: 7905032]

41. Horwood JM, Dufour F, Laroche S, Davis S. Signalling mechanisms mediated by the phosphoinositide 3-kinase/Akt cascade in synaptic plasticity and memory in the rat. Eur J Neurosci. 2006; 23:3375–84. [PubMed: 16820027]

42. Sutton G, Chandler LJ. Activity-dependent NMDA receptor-mediated activation of protein kinase B/Akt in cortical neuronal cultures. J Neurochem. 2002; 82:1097–105. [PubMed: 12358757]

43. Elias GM, et al. Synapse-specific and developmentally regulated targeting of AMPA receptors by a family of MAGUK scaffolding proteins. Neuron. 2006; 52:307–20. [PubMed: 17046693]

44. Zimmermann P. The prevalence and significance of PDZ domain-phosphoinositide interactions. Biochim Biophys Acta. 2006; 1761:947–56. [PubMed: 16884951]

45. Heo WD, et al. PI(3,4,5)P3 and PI(4,5)P2 lipids target proteins with polybasic clusters to the plasma membrane. Science. 2006; 314:1458–61. [PubMed: 17095657]

46. Jin W, et al. Lipid binding regulates synaptic targeting of PICK1, AMPA receptor trafficking, and synaptic plasticity. J Neurosci. 2006; 26:2380–90. [PubMed: 16510715]

47. Campbell RE, et al. A monomeric red fluorescent protein. Proc Natl Acad Sci U S A. 2002; 99:7877–82. [PubMed: 12060735]

48. Phend KD, Rustioni A, Weinberg RJ. An osmium-free method of epon embedment that preserves both ultrastructure and antigenicity for post-embedding immunocytochemistry. J Histochem Cytochem. 1995; 43:283–92. [PubMed: 7532656]
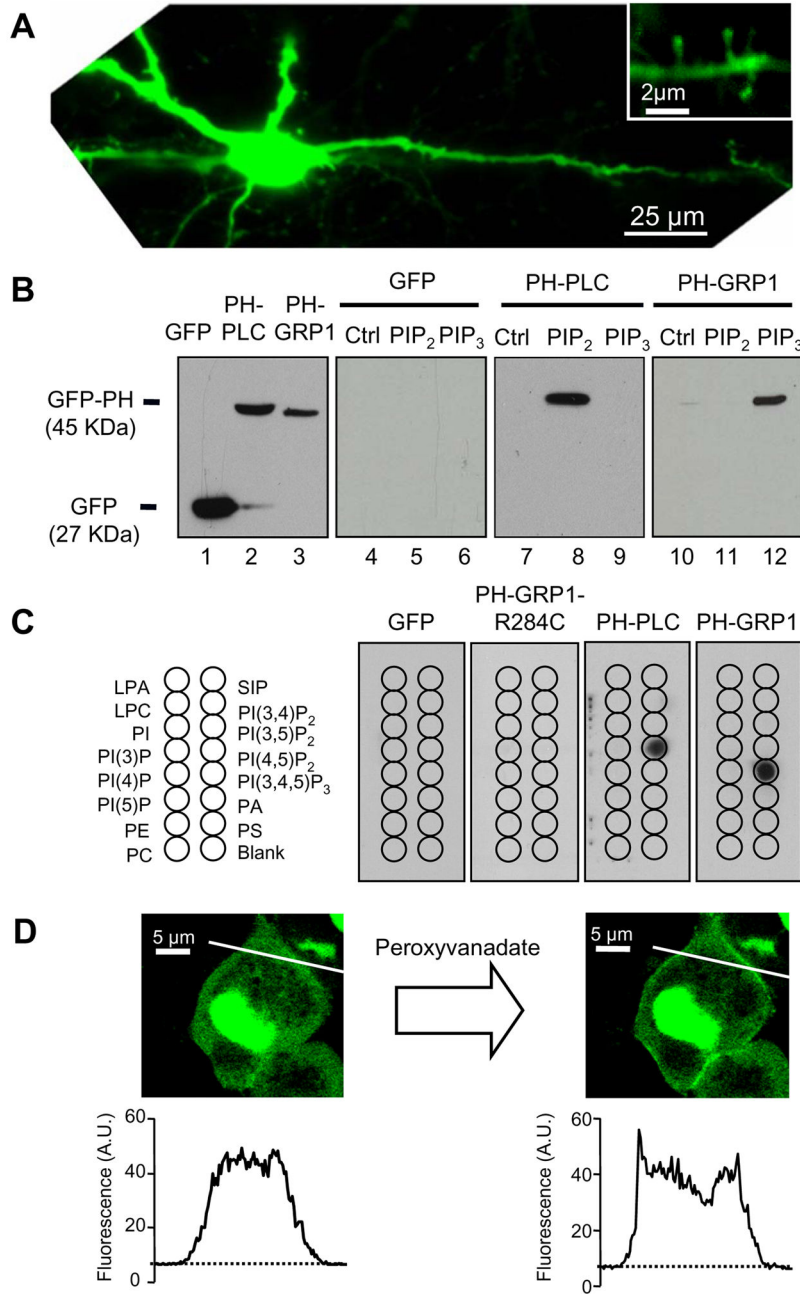
Figure 1. Expression of PH-GRP1 in hippocampal neurons and specific binding to PIP$_3$
A Expression of PH-GRP1-GFP in the soma, dendrites, and dendritic spines (inset) of CA1 pyramidal neurons in organotypic cultures. **B**. Protein extracts from hippocampal slices expressing GFP (lanes 1, 4–6), GFP-PH-PLC (lanes 2, 7–9), or GFP-PH-GRP1 (lanes 3, 10–12) were incubated with agarose beads (Echelon) covalently linked to PIP$_2$ (lanes 5, 8, 11), PIP$_3$ (lanes 6, 9, 12), or control beads (lanes 4, 7, 10). Pull down fractions were analyzed by western blot with anti-GFP antibody (Roche). Input extracts: lanes 1–3. **C.** Similar extracts to those used in (B) were incubated with membranes spotted with an array of different phospholipids and phosphoinositides (see http://echelon-inc.com for a full list of lipid

abbreviations). Membrane bound fractions were visualized with anti-GFP (Roche). **D.** Representative example of BHK cells expressing GFP-PH-GRP1 before (left) and after (right) stimulation with peroxyvanadate (5 min incubation with 30 μM peroxide, 100 μM ortho-vanadate). Line plots show quantification of fluorescence intensity across the cell. Note accumulation of GFP-PH-GRP1 at the cell edge (plasma membrane) after stimulation.
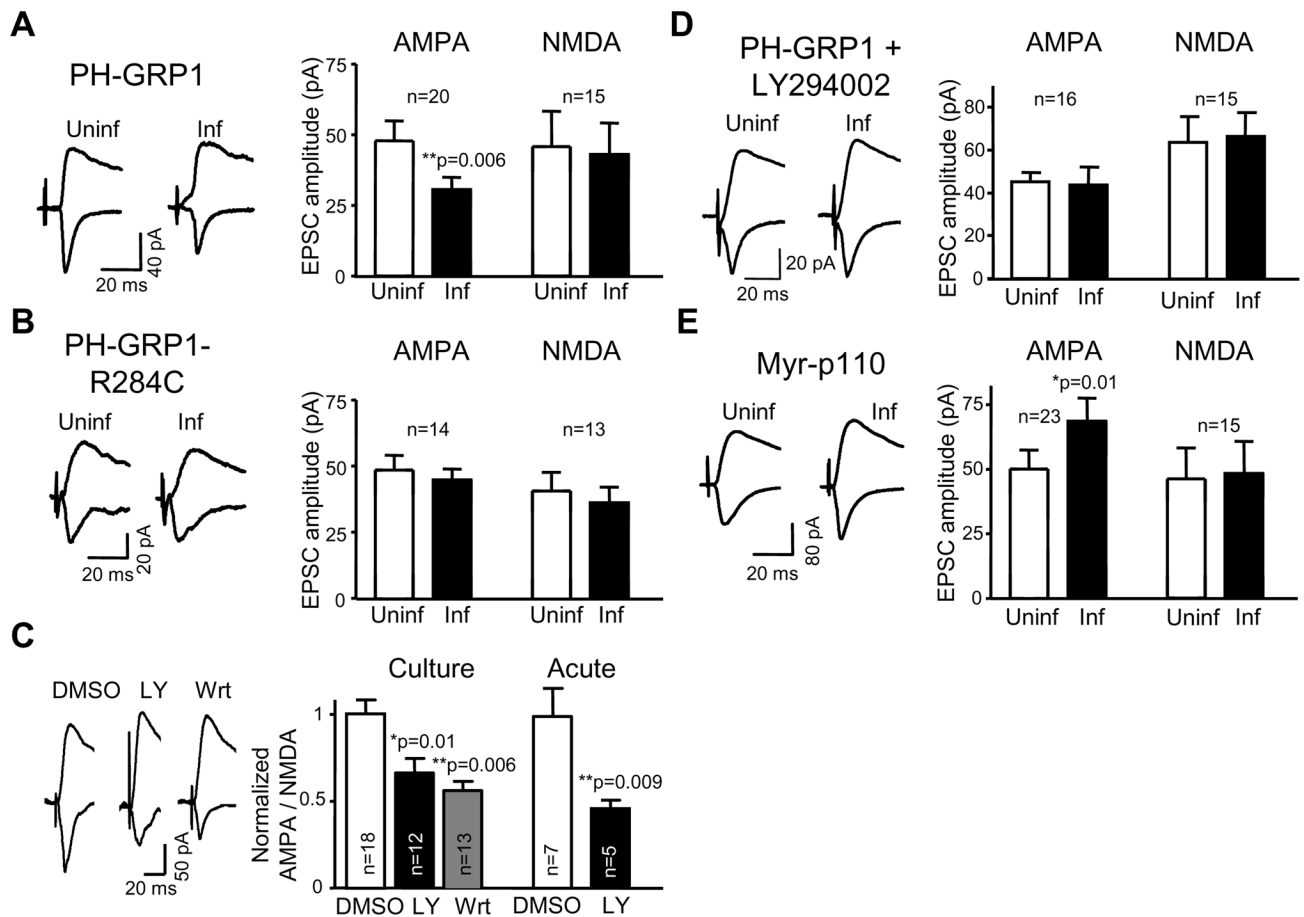
Figure 2. Bidirectional modulation of AMPA-receptor mediated currents by PIP$_3$

A, B, D, E Comparison of evoked synaptic responses from pairs of neighboring CA1 neurons expressing PH-GRP1 (**A, D**), PH-GRP1-R284C (**B**) or Myr-p110 (**E**), and control (uninfected) neurons recorded at −60 mV (AMPAR EPSCs) and +40 mV (NMDAR EPSCs). Some slices were pre-treated for 1 hour with 10 μM LY-294002 (**D**). Example traces from uninfected and infected neurons are shown on the left for all panels. "n" represents number of cell pairs. Statistical significance was calculated according to the Wilcoxon text for paired data (individual pairs of infected *versus* uninfected cells). **C.** Comparison of evoked synaptic responses from CA1 neurons pre-treated for 1 hour with 10 μM LY-294002 ("LY") or 100 nM wortmannin ("Wrt") or with the vehicle control (0.05% DMSO). The AMPA/NMDA ratio is calculated from the size of the AMPAR- and NMDAR-mediated responses recorded at −60 mV and +40 mV, respectively. Experiments were carried out on organotypic cultured slices (left histrogram) or on acute slices (14 days postnatal; right histogram). Representative traces are shown on the left. "n" represents number of cells; "p" values were calculated according to the Mann-Whitney test. In all cases, error bars represent s.e.m.

Figure 3. Inhibition of PIP$_3$ synthesis produces a slow and gradual depression of AMPA receptor-mediated transmission

A. Examples of evoked field excitatory postsynaptic potentials (fEPSP) obtained from hippocampal slices 5–25 minutes before ("baseline") or 120–140 minutes after ("120–140") treatment with DMSO (left) or 10 μM LY294002 (right). Presynaptic fiber volleys and fEPSPs are indicated with arrows. **B.** Time course of the slope of fEPSP responses from hippocampal slices treated with 10 μM LY294002 (black symbols) or DMSO (white symbols) (drug application is shown with a black bar). Values are normalized to the average slope before drug application. "n" represents number of slices. Statistical significance for the

comparison between DMSO- and LY294002-treated slices was done according to the Mann-Whitney test. **C.** The amplitude of the presynaptic fiber volley was analyzed from the experiments shown in B. Values are normalized to the average fiber volley amplitude before drug application. No significant change in fiber volley amplitude was observed over the time course. **D.** Time course of whole-cell currents recorded from CA1 pyramidal neurons infected with PH-GRP1 (black symbols) or uninfected control neurons (white symbols) during the application of 100 nM AMPA (bar). "n" represents number of cells. In all cases, error bars represent s.e.m.
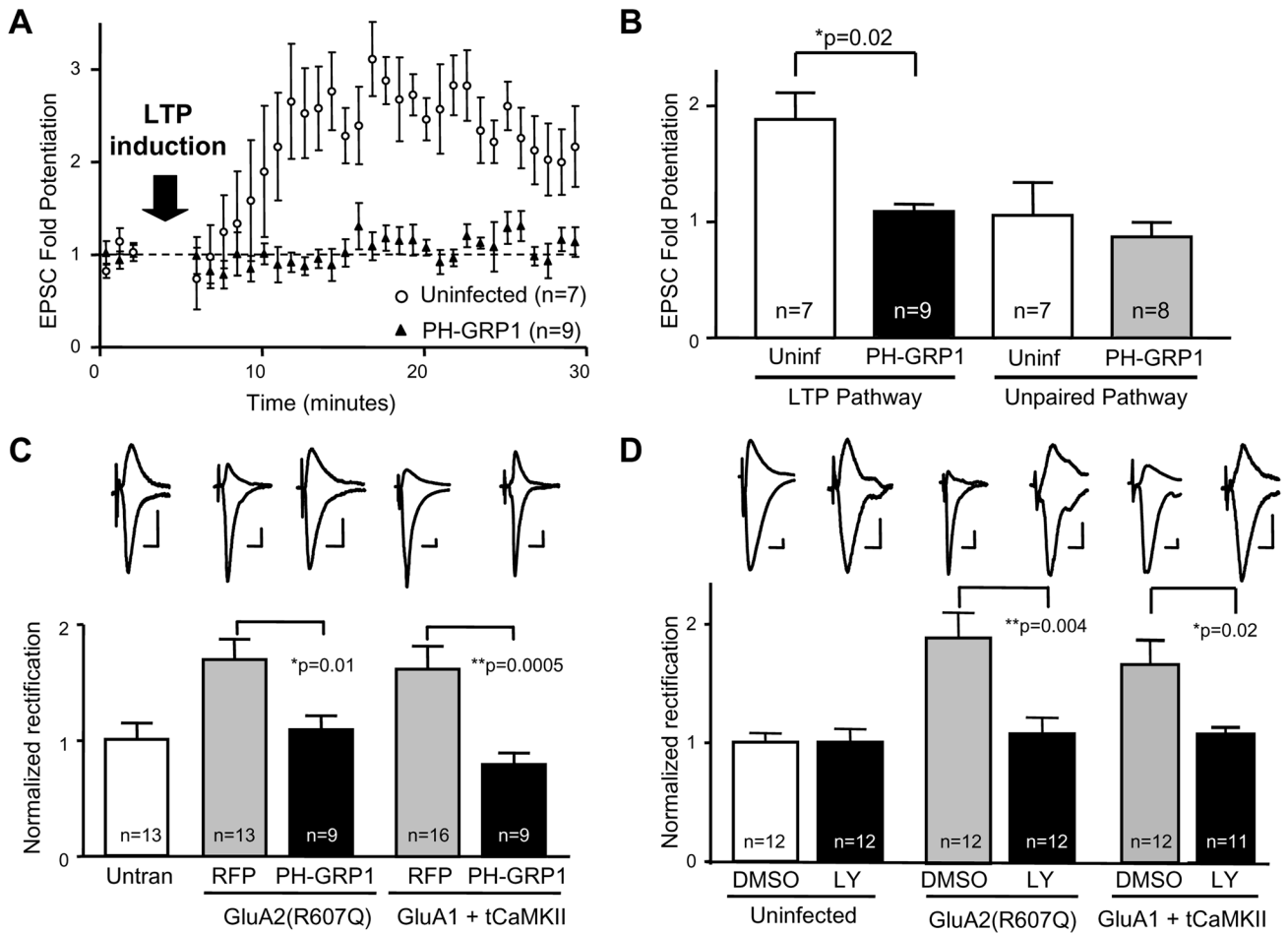
Figure 4. PIP₃ is required for LTP and it affects both constitutively cycling and regulated populations of AMPA receptors

A. Time course of AMPAR-mediated synaptic responses before and after LTP induction (black arrow) in control (uninfected) CA1 neurons (white symbols) and in PH-GRP1-expressing cells (black symbols). **B.** Quantification of average synaptic potentiation ("LTP Pathway") from the last 5 min of the time course shown in A. One of the stimulating electrodes was turned off during LTP induction ("Unpaired Pathway"). **C.** CA1 neurons were transfected with different combinations of GluA2(R607Q) or GluA1 plus constitutively active CaMKII (tCaMKII), together with RFP or RFP-PH-GRP1 coexpression, as indicated. Synaptic responses were evoked at −60 mV and +40 mV to quantify inward rectification. Rectification indexes were normalized to the average value obtained from untransfected cells (2.0 ± 0.3). Representative traces of the recordings are plotted above their respective columns in the graph (scale bars: 20 pA, 10 ms). **D.** Similar experiments as in C, with the indicated recombinant proteins and slices treated with 10 μM LY294002 or DMSO (vehicle control) for 1 hour (LY294002 and DMSO were also present during the recordings). Rectification index for uninfected, DMSO-treated cell was 2.4 ± 0.2. Representative traces of the recordings are plotted above their respective columns in the graph (scale bars: 20 pA, 10 ms). In all cases, "n" stands for the number of cells, error bars

represent s.e.m. and statistical significance was calculated according to the Mann-Whitney test.
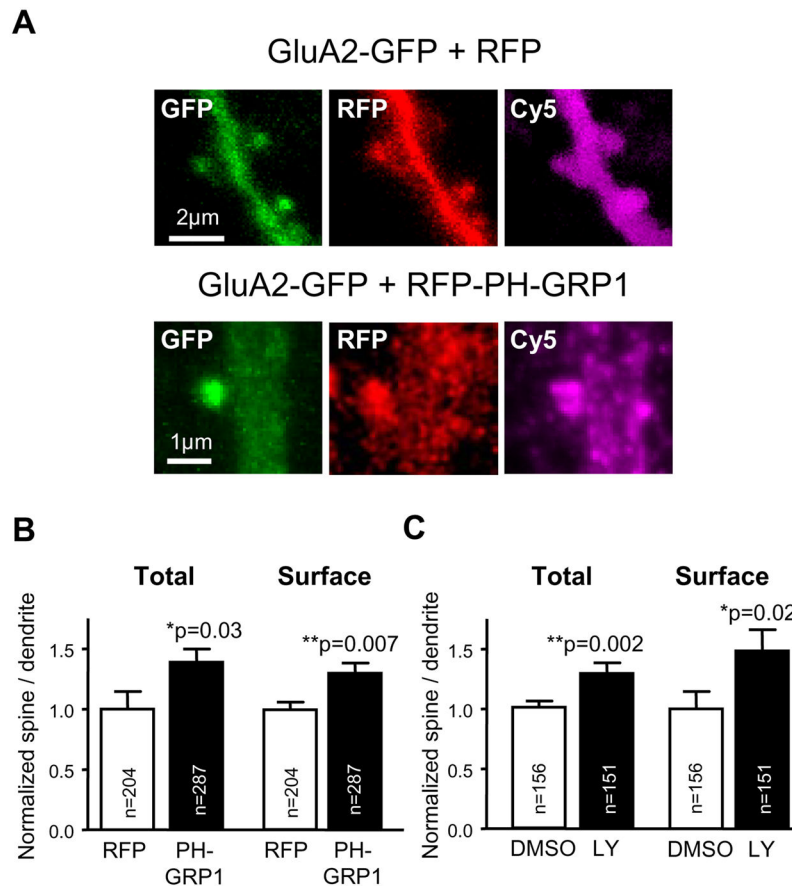
Figure 5. Depletion of PIP$_3$ leads to the accumulation of AMPA receptors in dendritic spines
A Representative confocal images of total receptor ("GFP", green) and surface anti-GFP labeling ("Cy5", purple) in dendritic spines from neurons expressing GluA2-GFP with RFP (top panels) or with RFP-PH-GRP1 (bottom panels). **B**. Quantification of fluorescence intensity at spines versus the adjacent dendritic shaft from neurons as those shown in A. "Total Receptor" (left) is quantified from GFP fluorescence, and "Surface Receptor" (right) from Cy5 signal. Values of spine/dendrite ratios are normalized to the control (RFP-expressing neurons). The actual (non-normalized) ratios for the control were (average ±s.e.m.): 1.15 ±0.2 (total) and 1.0 ± 0.1 (surface). "n" represents number of spines from 11 (GluA2 + RFP) or 25 (GluA2 + PH-GRP1) different neurons. Statistical significance was calculated according to t test. **C.** Neurons expressing GluA2-GFP were treated with 10 μM LY294002 or DMSO (vehicle control) for 1 hour prior to fixation and imaging. Total and surface receptors are plotted as in B. Values of spine/dendrite ratios are normalized to the control (DMSO-treated neurons). The actual (non-normalized) values for the control were (average ± s.e.m.): 1.5 ±0.1 (total), 1.1 ±0.2 (surface). "n" represents number of spines from 25 (DMSO) or 22 (LY294002) different neurons. Statistical significance was calculated according to t test.
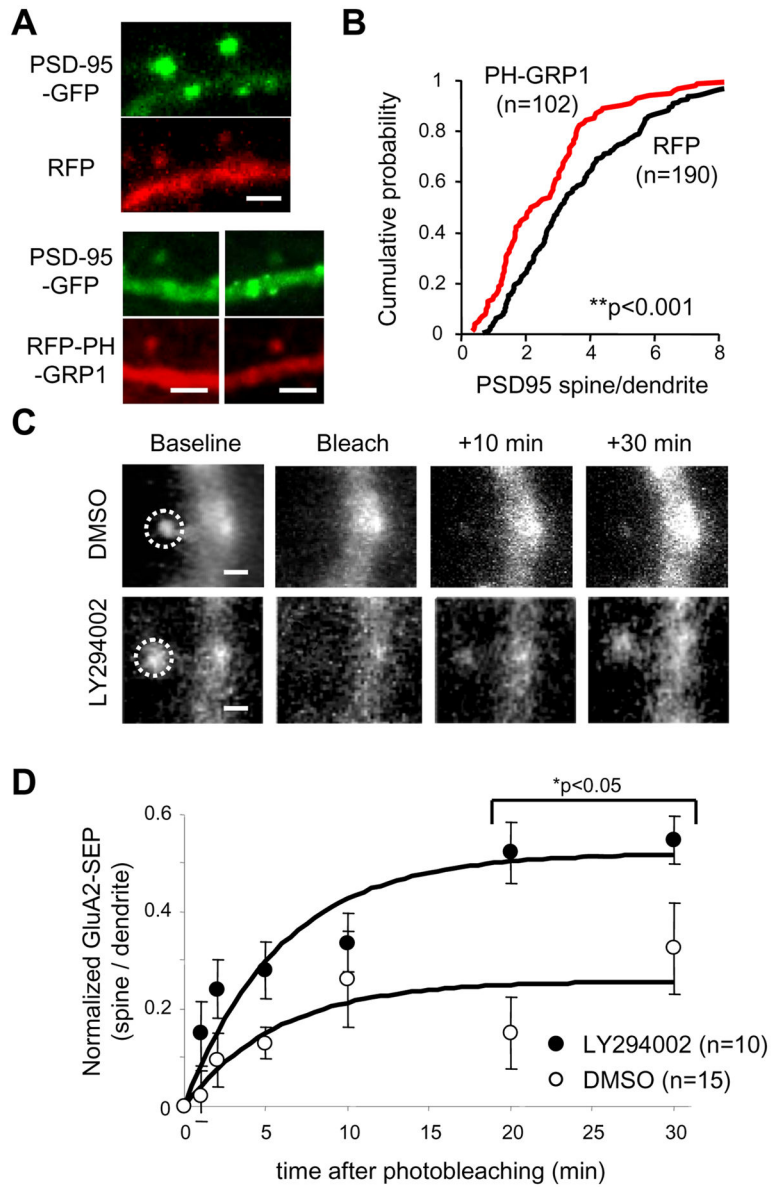
Figure 6. Depletion of PIP$_3$ impairs PSD-95 accumulation in spines and increases surface mobility of GluA2 recombinant receptors

A. Representative confocal images of dendritic spines from neurons expressing PSD-95-GFP (green images) with RFP (top panels) or with RFP-PH-GRP1 (bottom panels). **B**. Quantification of fluorescence intensity at spines versus the adjacent dendritic shaft from neurons as those shown in A. "n" represents number of spines from 29 (PSD-95 + RFP) or 12 (PSD-95 + PH-GRP1) different neurons. Data are presented as cumulative distributions of spine/dendrite ratios (average spine/dendrite ratio ± s.e.m. was 3.7±0.15 for PSD-95 + RFP, and 2.6±0.15 for PSD-95 + PH-GRP1). Statistical significance is calculated according to the Kolmogorov-Smirnov test. **C.** Examples of spines expressing GFP-GluA2, treated with either DMSO (vehicle) or 10 μM LY49002 for 1 hour prior to undergoing a FRAP experiment. Representative images are shown before photobleaching ("Baseline"), right after photobleaching ("Bleach") and at different times during fluorescence recovery, as

indicated. Bleached regions are indicated with dashed circles in the "Baseline" panels. **D.** Quantification of the amount of GluA2-GFP fluorescence at the spine normalized to the baseline value before photobleaching. Fluorescence intensity at the spine is normalized to the adjacent dendrite (spine/dendrite ratio) to compensate for ongoing photobleaching during image acquisition. Time courses obtained from DMSO- (white symbols) or LY294002-treated slices (black symbols) were fitted to single exponentials (solid lines). Best-fit parameters were: τ=5.7 min, amplitude=0.26 (DMSO); τ=5.9 min, amplitude=0.52 (LY294002). Correlation coefficients were 0.71 (DMSO) and 0.84 (LY294002). Error bars represent s.e.m.
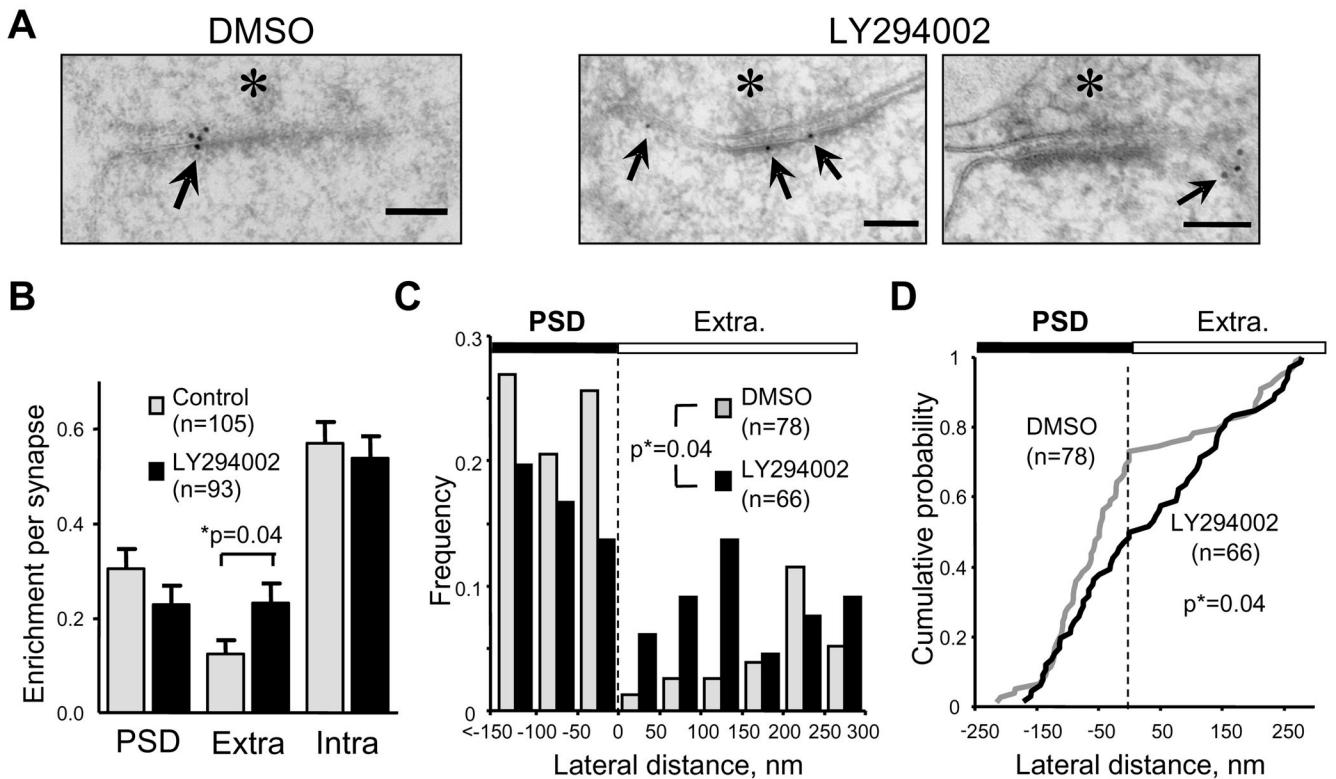
Figure 7. Depletion of PIP$_3$ causes a redistribution of AMPARs between the PSD and extrasynaptic membrane

A. Examples of electron micrographs from CA1 excitatory synapses labeled with anti-GluA2 immunogold (arrows). Presynaptic terminals are indicated with asterisks. Slices were treated with either DMSO (vehicle) or 10 μM LY294002 for 1 hour before fixation. Scale bars represent 100 nm. **B.** Quantification of GluA2 immunogold abundance at the PSD, the extrasynaptic membrane ("Extra") or the intracellular space ("Intra") from slices treated with DMSO (grey columns) or LY294002 (black columns). The number of gold particles at each compartment for a given synapse was divided by the total number of gold particles in that synapse. Average values ± s.e.m. are plotted for each compartment. "n" represents number of synapses analyzed. Statistical significance is calculated with the Mann-Whitney test. **C**. Frequency histogram of the lateral distribution of GluA2 immunogold particles contained within the PSD or the extrasynaptic membrane. Lateral distances are calculated for individual gold particles with respect to the closest PSD edge, with negative distances for particles within the PSD and positive distances for particles within the extrasynaptic membrane. Only particles within 290 nm (average PSD length) were considered for this analysis. Values are plotted for DMSO- (grey) and LY294002-treated slices (black). "n" represents number of gold particles. Statistical significance was calculated with a χ^2 test (contingency table). **D.** The same values shown in C are plotted as cumulative distributions. "n" represents number of gold particles. Statistical significance is calculated with the Kolmogorov-Smirnov test.
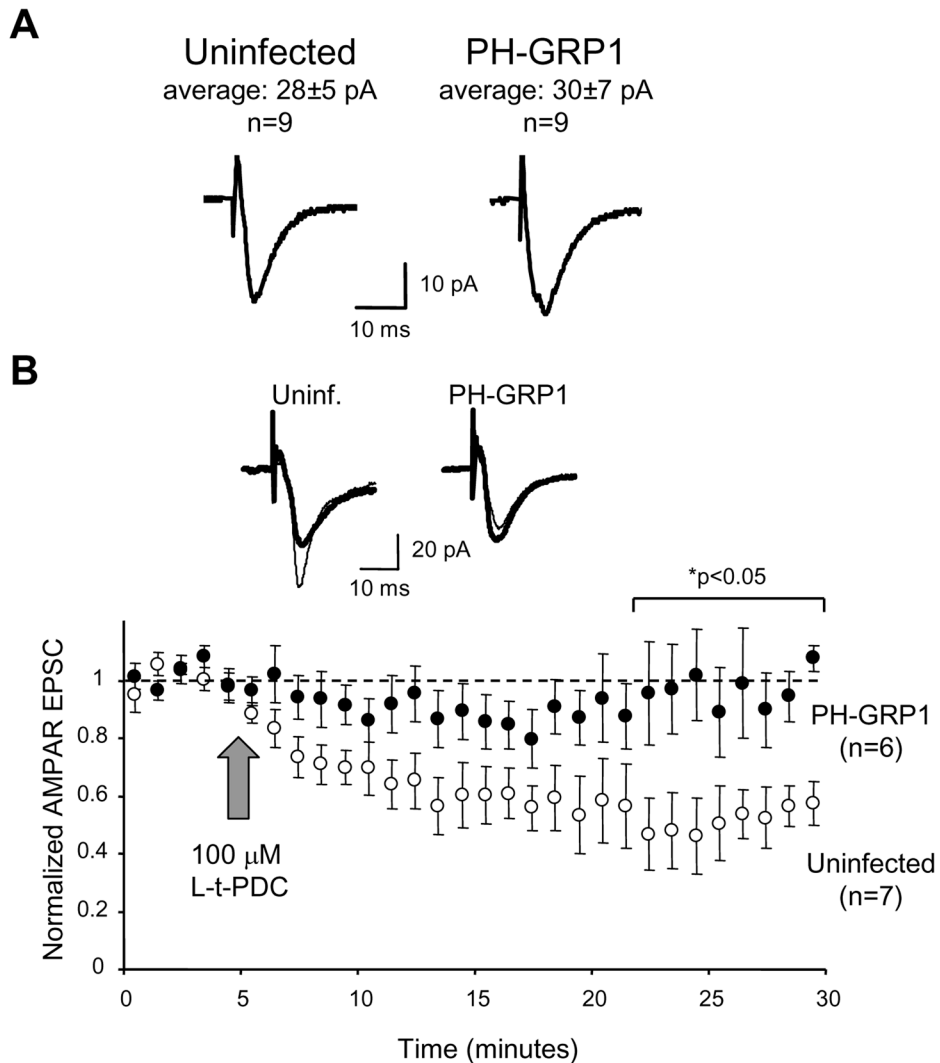
application. Thin lines: average response before L-t-PDC application. Thick lines: average response from the last 5 min of the time course.